STUDIES IN ROCK FRACTURE

John Handin

Texas A and M University

Prepared for:

Corps of Engineers (Army)
Advanced Research Projects Agency

29 December 1972

a report

from the Texas A&M
RESEARCH FOUNDATION
College Station, Texas

STUDIES IN ROCK FRACTURE

John Handin

Center for Tectonophysics
Texas A&M University
College Station, Texas

Contract No. DACA73-68-C-0004

WORK SPONSORED BY ADVANCED RESEARCH PROJECTS AGENCY

DEPARTMENT OF DEFENSE

ARPA Order No. 1074 Amendment 6

FINAL REPORT

Period covered: November 1, 1967 - October 31, 1972

Technical Monitor: R. W. Bruhn

Distribution of this document
is unlimited

December 29, 1972

Prepared
for

Department of the Army
Omaha District Corps of Engineers
U.S. Post Office and Courthouse
Omaha, Nebraska

INTRODUCTION

The overall objective of this project, "Studies in Rock Fracture," has been to acquire a better understanding of the processes of fracture in rocks, needed in engineering rock mechanics, structural geology, and seismology. This project has involved an integrated program of theoretical, experimental, and field studies designed to improve the knowledge of why, when, where, and how fracturing occurs. It has been under the overall supervision of the Principal Investigator, J. Handin, and for purposes of planning and reporting it has consisted of three tasks:

Task 1, "Studies of Residual Strain," has been directed by M. Friedman who has been responsible for the measurements of residual strain as well as the petrofabric work on specimens provided by the rock properties tests of Task 3. Other staff who have contributed to Task 1 are G. Alani, J. M. Logan and D. W. Stearns. A. Brown was a research associate during the summers of 1968-1971.

Task 2, "Photomechanical Modeling," has been directed by G. M. Sowers. This task was suspended from 1 May 1968 to 31 October 1969 while the work was supported by a grant from the National Science Foundation. It was reinstated on 1 November 1969 and terminated on 31 October 1970.

Task 3, "Fast Strain-Rate Testing," has been directed by J. M. Logan with contributions by M. Friedman, J. Handin, and J. N. Magouirk.

Significant contributions have been made by several graduate research assistants: J. Coyne, J. J. Gallagher, J. Humston, T. Iwasaki, T. C. Nichols, Jr., H. S. Swolfs, and R. Vincent.

Because almost all our results have been published in detail in the nine Technical Reports and/or in scientific journals (see Appendix A),

the sponsor, the Advanced Research Projects Agency, and the contract monitor, the U.S. Army Corps of Engineers--Missouri River Division, have agreed that this final report will only summarize our significant contributions. The single exception is the later work of Task 3 which has appeared only in quarterly progress reports and which is gathered here.

TASK 1. STUDIES OF RESIDUAL STRAIN

Introduction

Applications of rock mechanics to the design of engineering structures in rock and to structural geology involve the assumption that in situ stresses are due entirely to the present applied loads. For instance, one assumes that the vertical normal stress in undisturbed rock is equal to the weight per unit area of the overburden. In fact, vertical normal stresses of more than 100 times the present overburden pressure have been measured by strain-relief methods. The notion of residual stress seems unassailable, and indeed it has long been recognized by metallurgists. In fact, the in situ elastic strain energy measured by strain-relief techniques results from the superposition of present natural loading, present loads induced by man, and loads induced by past tectonic events, i.e., the paleo-stresses.

The principal objectives for this task have been:

1. To compare the state of residual elastic strain detected by X-ray diffractometry with the state of in situ strain determined by strain-relief methods in order to acquire a better understanding of just what is being measured in the field by many workers in rock mechanics.

2. To evaluate the state of residual elastic strain ("prestrain") as an anisotropy capable of influencing the mechanical properties of rock, especially ultimate strength and fracture orientation.

3. To evaluate the state of residual elastic strain as a source of potential energy in fracture propagation.

4 To investigate the processes by which elastic strain is stored in rocks.

General

The overall effort and general conclusion of this task, presented in the fifth Technical Report and in Publications 3 and 4, are summarized here. Following are brief reports of the important subtasks that have contributed to our general understanding of residual strain in rocks.

Residual elastic strains (stresses) occur in rocks that have no external loads across their boundaries. The strains are stored by cementation and by certain other physical and chemical interactions between anisotropic grains while under load. In situ states of stress result from superposition of applied loads on the residual stress.

Facts about residual stresses obtained primarily from X-ray diffraction studies but supported by available data from strain-relief techniques include the following: (1) Magnitudes can be large; differential stresses between 300 and 400 bars have been measured in quartzites, sandstones, and granites. (2) Residual stresses relating to Mesozoic and possibly even to Precambrian geologic events have been mapped. (3) Principal axes of the prestress correlate with the geometry of large-scale folds and to stresses inferred from nearby fractures and calcite twin lamellae. (4) Residual stresses have been found to vary systematically along fault surfaces in such a manner as to be related to the process of sliding. Items (1-4) suggest that rocks have long-term fundamental strength; volumetric stored strain energy is commonly of the order 10^4 ergs/cm^3. (5) Stored stresses relax when grains are freed from constraints of nearest

neighbors. (6) They relax within 5 mm of an induced tensile fracture in sandstone probably because movements along grain boundaries occur that far from the fracture surface. (7) Residual stresses influence the orientations of tensile and shear fractures induced experimentally under certain conditions of loading. (8) Prestresses can contribute to strength anisotropy. Items (7 and 8) are explicable from superposition of applied loads on residual stresses. (9) In the Barre granite the principal axes of residual strain are subparallel to the principal directions of ultrasonic attenuation and velocity fields.

The Influence of Residual Stress on Tensile and Shear Fracturing

This study has been to evaluate the influence of residual elastic strain on the orientations of tensile and shear fractures in rock. As a first step the three-dimensional state of residual elastic strain was measured by X-ray diffractometry in each of three quartzose sandstones. A prediction was then made concerning the orientations of fractures that would be induced in each rock by loading normal to bedding. The prediction was based upon a knowledge of the prestrain, the applied loads, and the maximum-tensile-stress and Coulomb-Mohr criteria. Each prediction was then tested by experimentally fracturing the rocks. Tensile fractures, induced in discs of Tennessee sandstone and Uinta Mountain quartzite by point-loading normal to bedding, exhibit a marked preferred orientation. Also strongly oriented are shear fractures induced in triaxial compression tests on cylinders of Tennessee sandstone (to 2000 bars confining pressure), Uinta Mountain quartzite (1500 bars) and Tensleep sandstone (1000 bars). In each rock the tensile fractures are parallel to the shear fractures

and both follow the predicted trend. To identify other possible causes for the fracture anisotropy, (a) apparent grain elongation, especially the trend of long axes within the bedding plane, (b) orientation of grain boundaries, (c) crystallographic orientation of quartz grains, and (d) orientation of quartz microfractures and deformation lamellae were investigated. All aspects of the fabric are randomly oriented except the trend of apparent long axes. The induced fractures cut across the trend of the long axes in two of the three rocks. It is concluded that the state of prestrain is controlling the orientations of the fractures. The anisotropy manifest by the prestrain persists to at least moderate confining pressures. (Technical Report No. 1 and Publications 5 and 6).

Photomechanical Model Studies of Fracture and Residual Elastic Strain in Granular Aggregates

A fundamental understanding of the relation between stress concentrations at grain contacts and microfractures in granular aggregates is obtained through two-dimensional photomechanical model studies and is tested through observations of experimentally deformed sandstone discs, glass beads, and quartz sand.

In uncemented aggregates, the stress state in each grain appears to be controlled by the manner in which the applied load is transmitted across grain contacts. The angles between lines connecting pairs of contacts and the axis of the principal load acting at the boundaries of the aggregate determine which of all contacts will be most highly stressed or "critical." Microfractures follow that maximum principal-stress trajectory which connects critical contacts, and they propagate through those points where the magnitude of the local maximum stress difference is the greatest.

Microfractures, therefore, are extension fractures. It then follows that both the locations and orientations of fractures can be predicted if the state of stress in the grains is known. This constitutes an extension-fracture criterion.

Positioning of critical contacts depends primarily on sorting, packing, grain shapes, and the boundary-load conditions on the aggregate. Some critical contacts and, therefore, microfractures tend to join together in a series or "chain." Orientations of chains are most strongly influenced by the direction of the maximum compressive load at the boundary of the aggregate.

A hydrostatic load applied on the boundaries of an aggregate can cause microfracturing within grains. Orientations for microfractures and contact lines are random in poorly sorted aggregates, but they are influenced by packing in well sorted aggregates.

Grains of aggregates cemented while unloaded are, upon later loading, more highly stressed at their centers than at contacts. By analogy, microfracture orientations depend strongly on the position of the greatest load axis and only slightly on the low-magnitude stress concentrations at contacts. These microfractures parallel the greatest principal-stress trajectory in regions where the magnitude of the maximum stress difference is greatest. These observations lead to the conclusion that fractures in grains of cemented aggregates are also extension fractures.

These conclusions hold when cementing materials have about the same elastic moduli as the grains. Cements may be so weak that the aggregate behaves as if it were uncemented in terms of microfracture fabric, or so strong that the major part of the load is transmitted by the cement, and

the composite is no longer an aggregate in the mechanical sense.

Aggregates cemented under load may contain stored elastic strain (stress) even close to a free surface introduced after cementing. The modulus of the cementing material plays an important role in the stress-storing process. Weak cements cannot store stress in grains but strong cements preserve almost all the original stresses.

Residual stresses will within the grains change, but high stress concentrations near contacts do not change appreciably when boundary loads are removed after cementing with a strong material. In addition, removal of the boundary load causes the central regions of grains to become nearly isotropic as stress is transferred to the cement. This observation of a heterogeneous state of stress within a grain, as well as in the cement, leads to better understanding of X-ray data on residual strain. (Technical Report No. 3 and Publication 10).

Fracture-Surface Energy of Rocks

Effective fracture-surface energies γ_{eff}, as determined from stable tensile fracture tests on a variety of rock types, are of the order of 10^4 ergs/cm^2 in contrast to values for constituent crystals which are 10^3 to 10^3 ergs/cm^2. The major source of discrepancy has been ascribed to improperly accounting for the entire new surface created by the propagation of fractures through granular media. One aspect of our continuing investigation of residual elastic strain in rocks has been the assessment of the contribution of such strain to the process of fracturing. Although the work is incomplete, it has confirmed this reason for these order of magnitude differences in single-crystal and rock values. From X-ray diffraction studies of changes in residual strain adjacent to tensile fractures in sandstone and also from thin-section studies of stained specimens, we

conclude that intergranular displacements take place in a region as much as 5 mm wide on each side of the fractures. When the total surface area of the grains within this region is equated to the total effective area of fracture created, γ_{eff} is reduced to the same order as that for single crystals. (Technical Report No. 4 and Publication 9).

Strains Associated with Relaxations of Residual Stresses upon Overcoring Granite in the Laboratory

A cube of Barre Granite (approximately 22 cm on a side), free of boundary loads, was sequentially and concentrically overcored with 5.1, 10.1 and 15.0-cm corebits on the "top" and "bottom" sides and with a 10.1-cm core bit on a "third" side. The top and bottom sides are parallel to the "grain" plane, which is horizontal in the quarry, and the third side is parallel to the "rift" plane, which is vertical and strikes N30°E. Strains resulting from overcoring were recorded on these sides with three arrays of 45°-rosette, resistance strain gages; there were 36 rosettes in all.

The strain changes observed upon coring seem to have been derived from a complexly changing internal (residual) stress field. Initially, as the top surface was overcored, the resulting strain changes were mostly compressional, i.e., the block contracted. These became more extensional as the bottom of the block was overcored. Finally, there were large net strain changes that were radially compressional and tangentially extensional relative to each set of concentric overcores.

The largest strain changes were observed adjacent to freshly cut surfaces, yet significant changes were monitored over the entire surface for each overcore. Strain changes monitored on opposing gages symmetrically

located across a freshly cut surface were generally similar in sense, magnitude, and direction.

The residual stress field is relatable to the changing geometry of the body, induced free surfaces, and to the degree of homogeneity, orientations, and magnitudes of the stresses when they were frozen in. Cumulative strain changes at individual gage locations were large, as much as 330×10^{-6} (extension) and -275×10^{-6} (compression).

The deformation generally appears to be elastic. At certain gages, however, there were occasional large, anomalous, strain changes that are interpreted to result from permanent deformations like intergranular movements or intragranular gliding. These mechanisms may also be in part responsible for a pronounced creep event that was observed after the top 15.0-cm coring was completed; i.e., the whole block, which had initially contracted, expanded for 48 hours after the coring event until the net strain change was nearly zero.

The deformations typically occurring across a pilot borehole as a result of stress-relief overcoring techniques can be caused by either a tensile residual stress field or an externally applied compressional stress field. (Technical Report No. 6).

In Situ Strain Measurement by Photoelastic Bar Gages

It may be possible to gain new insight into the mechanics of geologic structures from knowledge of the in situ strain (or stress) stored in deformed rocks. Many papers have been published on the techniques available for the measurement of in situ stress. Here it is sufficient to say that most measurements have been made for engineering purposes and that most techniques involve cumbersome equipment. We point out the advantages of

the photoelastic gaging method to the field geologist - simplicity and relatively easy portability.

Recoverable strain has been measured in situ with bridged, photoelastic bar gages, which have been satisfactorily tested against foil-resistance gages. Rosettes of 0.2 by 0.4 by 4-cm bars, bonded to the rock for 0.6 cm at each end, have been mounted on bedding planes and fracture faces. Change in strain is measured following overcoring with a 10-cm bit. Strains commonly lie between 10 and 200 x 10^{-6}, but values of over 1000 x 10^{-6} have been measured. Corrections for strains in the order of 30 x 10^{-6}/°C, due to differential thermal expansion between rock and gage, are made by monitoring dummy gages mounted on free blocks. The variations in strain change are large over a period of several days. In some cases the initial relief is related to tectonic deformation. Coaxially mounted rosettes show that the amount of recovery depends on the proximity to the freed surface. A partial relaxation of the strain, normal to a pervasive fracture set, may occur prior to an investigation, so that the major extension on overcoring is oriented parallel to such sets.

At Rangely, Colorado photoelastic data agree with measurements by five other methods, and are consistent with local fractures and the formation of the anticline. At three sites on Rattlesnake Mountain, Wyoming the strain recovery two weeks after overcoring is correlated with stresses thought to occur within such a block during asymmetric uplift. The orientations of recovery axes at two sites, 72 km apart, in the Llano region, Texas, are similar and are related to stresses during Paleozoic folding as well as the opening of fractures during uplift. (Technical Report No. 7 and Publications 1 and 2).

TASK 2. PHOTOMECHANICAL MODELING

The objectives of this task have been:

1. To provide a better mechanical explanation for the distribution of certain fractures in heterogeneously layered rocks so deformed that a maximum axis of extension lies in plane of bedding.

2. To develop an adequate theory that will permit the computation of critical loads for the initiation of instability and fracture of rocks in engineering activities such as tunneling

3. To provide an approximate basis for the computation of loads which caused certain geologic fractures.

4. To make experimental tests of the theory by photoelastic modeling methods.

The results are presented in Technical Report No. 9 (Appendix A), the final report of this task, which is summarized as follows.

A new theory of the spacing of extension fractures in flattened, or compressed, layered rocks provides a basis for predicting certain natural fracture patterns, and the theory is confirmed by model studies.

Fracture spacing may be controlled by elastic stress concentrations. In compressed layered rocks, the initial uniform stress field may become unstable, and periodic stress concentrations may develop. This instability is caused by differences in mechanical properties of the layered sequence causing incremental interfacial stresses as deformation goes on. A critical stress is required to initiate the instability. If the critical stress exceeds the rock strength, then fracture occurs according to older theories, but loads of equal magnitude can cause elastic instability in bodies of other shapes.

By using strain energy methods, a quantitative theory is developed. Work done in lengthening a stiff layer is computed and equated to the elastic strain energy of deformation. This energy is computed for the change in shape associated with the necking of the stiff layer and is then combined with the deformation energy computed for the loading of the restraining medium. When external work and strain energy so computed are equal, the necked shape is favored over the straight form which is the earliest stable shape in the deformation.

Different combinations of interfacial forces are used to obtain a measure of the effect of friction and welding at layer interfaces. Fracture spacing computed for these cases agrees well with experimental values. This theory may be applied in devising patterns of rock bolting and perhaps for setting charges in advancing rock faces in rapid excavations.

TASK 3. FAST STRAIN-RATE TESTS

Introduction

There has been a wide gap in our knowledge of the strain-rate spectrum between the fastest "static" tests (about 1 per second) and shock-tube and high-explosive testing (10^6 per second and higher). We have not known how rocks will respond to stress differences of a few kilobars acting for a few milliseconds. Phenomena associated with these intermediate strain rates range from the focal mechanisms of earthquakes to the transfer of energy from nuclear explosions into rocks. Thus a reconnaissance of the mechanical properties of rocks at rates of the order of 10^2 per second seems important.

The principal objectives for this task have been:

1. To design and build a fast strain-rate triaxial compression

tester for 2-cm rock specimens at confining pressures to 8 kb and temperatures to 400°C.

2. To test a wide variety of rocks at intermediate strain rates of 10^{-2} to 10^{2} per second, and to study the deformation mechanisms under these new conditions.

General

Apparatus design, testing techniques, and early results, presented in the second Technical Report and in Publication 13, are summarized here. Following are brief reports of the important subtasks that have contributed to our understanding of fracture in the laboratory, the results of which have been published. Finally, we present intermediate strain-rate data that have not been published.

Quasi-dynamic triaxial compression tests have been done for the first time at confining pressures to 7 kb. The intermediate strain-rate apparatus employs a gas loading cylinder which allows axial strain rates up to 10^{2}/sec on a sample 2 cm in diameter and 4 cm long. Samples can be deformed at confining pressures to 7 kb. Strain gages bonded to the loading piston and to the jacketed specimen allow internal measurements of load and sample strains respectively.

Westerly granite has been deformed at confining pressures to 7 kb, room temperature, and axial strain rates of 10^{-2} to 1/sec. An increase of ultimate strength with confining pressure was found as expected. The ultimate strength was also found to vary directly with increasing strain rate; the rate of rise increases with confining pressure. Brittle deformation has dominated the sample behavior.

Solenhofen limestone has been deformed at confining pressures to 3 kb, room temperature, and axial strain rates of 10^{-2} to 10/sec. The

brittle-ductile transition was found to take place at about 1.5 kb confining pressure at a strain rate of 10/sec.

Lueders' Bands in Experimentally Deformed Sandstone and Limestone

Planar deformation features inclined along planes of high shear stress and along which cataclasis is concentrated are here called Lueders' bands. In Coconino Sandstone (deformed dry and with pore pressure at effective confining pressures to 2.4 kb, room temperature, and at a strain rate of 10^{-4}/sec) the bands begin to develop in the transitional regime and are the major deformation feature in the macroscopically ductile regime. At axial shortenings of 5 percent and more they pervade the specimen and become closer spaced and thicker with increasing strain. In thin section the bands are formed by two or more layers of moderately to highly fractured quartz grains. They are markedly different from shear fractures (or faults) of similar size that typically contain quartz gouge. The average angle between conjugate sets of bands bisected by the greatest principal compressive stress σ_1 increases with effective confining pressure from 72° to 110°. The corresponding angles between conjugate macroscopic shear fractures averages 60°. The angle between Lueders' bands is essentially unchanged for increasing strain at fixed effective confining pressure.

In Solenhofen Limestone (deformed dry at confining pressures to 3.0 kb, 24°C, and strain-rates from 10/sec to 10^{-4}/sec) the bands are developed in the outer shell of the solid cylinders; however, in coarser grained limestones the bands are pervasive as in the sandstone. In cylinders of Solenhofen the bands are best developed in the transitional regime. They do not form in the ductile regime as gliding flow becomes the predominant mechanism

of deformation. The average angle between conjugate sets is independent of strain and strain rate; but as for the sandstone, it increases with confining pressure from 63° to 115°, and it is at least 20° larger than the corresponding angle between conjugate shear fractures which form after the bands. Optical and SEM studies indicate that the features in both rocks are zones of inter- and intragranular cataclasis, along which shear displacements are negligible.

Because the angle between conjugate Lueders' bands is a function of the effective confining pressure, the bands might be used to define depth of burial at time of deformation, provided that (1) the pore-fluid pressure is assumed to be hydrostatic, and (2) the orientation of σ_1, which can be the acute or obtuse bisector, is independently known. This approach is illustrated with reference to an occurrence of Lueders' bands in naturally deformed Entrada Sandstone, Trachyte Mesa, Utah. (Technical Report No. 8 and Publication 8).

Microscopic Feather Fractures

Certain microfractures adjacent to faults in experimentally deformed cylinders of Westerly Granite form as a result of shear displacement along the primary fault, and they are oriented consistently relative to the fault surface. These fractures are described in detail because they are: (a) symptomatic of a homogeneous state of stress in the region of the fault at the time of faulting; (b) criteria to demonstrate that shear displacement has occurred along a fault; and (c) criteria to establish unequivocally the sense of shear. (Publication 7).

Unpublished Intermediate Strain-Rate Data

"Wagonwheel" Graywacke. Our tests on this sandstone, which may be involved in a Plowshare experiment, were done in cooperation with H. C. Heard of Lawrence Livermore Laboratory who carried out the static tests at 10^{-4}/sec in his laboratory. Figure 1 shows the stress-strain curves for strain rates of about 5/sec and confining pressure to 6 kb. Inspection of the specimens deformed at 6 kb reveals no macroscopic fractures, that is the specimens are macroscopically ductile. The specimen deformed at 4 kb failed by faulting. The brittle-ductile transition at about 5 kb is much higher than that observed at a strain rate of 10^{-4}/sec, at about 1 kb confining pressure.

A comparison of these strain-rate data is shown in Figure 2. The points for both dry specimens and those 50-percent saturated with distilled water fall along the same curve. The increase of ultimate strength is 2-3 percent per decade of strain rate. The higher is the pressure, the greater is the effect of strain rate; the curves diverge. This same behavior had also been found in Westerly granite (Technical Report No. 2).

Berylluim Oxide. Also in cooperation with Heard, who made the tests at a strain rate of 10^{-4}/sec, we tested this material at about 20/sec and under 0-6 kb confining pressure (Figure 3). The brittle-ductile transition occurs between 24 and 26-kb mean pressure (confining pressures of 6 kb). At a strain rate of 10^{-4}/sec the transition is only about 13-kb mean pressure. Figure 4 is a plot of the shear stress versus mean pressure for the ultimate strength of each test. The increase of ultimate strength with strain rate is about 3 percent per decade of strain rate at the lower pressures and about 10 percent per decade at mean pressures of about 26 kb.

Cedar City "Tonalite." Specimens, 2 cm in diameter and 4 cm long, were deformed dry at room temperature at an average strain rate of about 2/sec (Figure 5). Crushing occurs in unconfined tests, but at confining pressures of 1 kb and higher, a single shear fracture forms at about 25° to the compressive load axis.

For comparison, tests at a strain rate of 10^{-4}/sec were done on 1 by 2-cm specimens in a different apparatus (see Technical Report No. 1, p. 29). This rock is brittle at confining pressures of 1 kb or less, and it appears to enter a regime of transitional behavior at about 2 kb (Figure 6). These data agree well with those of Brown and Swanson (1970, p. 75) for the same test conditions. A comparison of the ultimate strengths at strain rates of 10^{-4} and 2/sec (Figure 7) indicates that up to 2 kb confining pressure, the increase in strength is about 250 bars for a four-decade increase in strain rate. Above 3 kb the curves diverge so that the increase is as large as 1 kb. It appears that the framework of the tonalite is sufficiently strong that a confining pressure of at least 3 kb is needed to collapse most of the pore space. When most grains are in contact the tonalite begins to behave like the Westerly Granite.

Solenhofen Limestone. Data are available on this dry rock at confining pressures to 3 kb and strain rates of 10^{-4} to 10/sec. The data are scattered, especially at the higher strain rates, but from about 25 tests, consistent relations between strength, confining pressure, and strain rate have emerged (Figure 8). At all strain rates there is an increase of ultimate strength with confining pressure, although the increase is not linear. There is also an increase of ultimate strength with increasing strain rate, also non-linear. The brittle-ductile transition is affected

also by increasing the strain rate. At 10^{-4}/sec, this transition occurs at about 1.5 kb confining pressure. At 10^{-2}/sec, the transition is raised to about 2 kb, and at the fastest rates to 3 kb. This generally agrees with the behavior of Westerly Granite and Wagonwheel Graywacke. In contrast to Westerly granite, however, the initial slope of the stress-strain curve is unaffected by strain rate in agreement with Green and others (1971).

Coconino Sandstone. Triaxial compression tests have been done at strain rates of 10^{-4} to 1 per second and confining pressures to 4 kb on Coconino Sandstone specimens under the following conditions: (1) oven-dried at 115°C for 24 hours, (2) saturated with distilled water for 24 hours but with pore pressure maintained at atmospheric, and (3) water-saturated with pore pressures to 2.5 kb. Owing to the limited amount of starting material, specimens for conditions 1 and 2 were cored from one block and those for condition 3 from another block, so that lithologic differences must be accounted for.

The stress-strain curves for a strain rate of 10^{-4}/sec are shown in Figure 9. The rock fails by fracture up to a confining pressure of 1.7 kb where faulting occurs. At 2.4 kb cataclasis occurs, and the specimen deforms in a microscopically ductile fashion. Three strain rates, differing by a maximum of 5 orders of magnitude, have been investigated. Ultimate strength increases with strain rate (Figures 9, 10, 11). This is consistent with our previous work on Westerly granite and Wagonwheel Graywacke. There is no consistent change of elastic modulus with strain rate.

Water-saturated specimens were tested at an average strain rate of 10^{-2} per second, and their behavior is indistinguishable from that of the dry samples (Figure 12).

During pore-pressure tests the internal water pressure is monitored by an oscilloscopic record of the water-pressure transducer. The average strain rate was 10^{-1} per second (Figure 13). To be certain of comparison, tests on dry samples from the same block were also run at 1 kb confining pressure. The Terzaghi effective-stress law appears to hold; ultimate strength is a function of the difference between external confining and internal pore pressures. However, at these rather high strain rates, the pore pressure increases slightly as the deformation progresses, presumably because compaction occurs so rapidly that the pore pressure can not equilibrate. The rock should tend to work soften as the effective pressure is decreasing.

References Cited

Brown, W. S. and Swanson, S. R., 1970, Constitutive equations for Westerly granite and Cedar City tonalite for a variety of loading conditions: Final Report, Defense Atomic Support Agency, DASA-2473.

Green, S. J., Leasia, J. D., Perkins, R. D., Jones, A. H., 1971, Multiaxial stress behavior of Solenhofen Limestone and Westerly granite at high strain rates: Terra Tek, Inc., Report TR71-10.

APPENDIX A

List of Technical Reports

1. "The Influence of Residual Elastic Strain on the Orientations of Experimental Fractures in Three Quartzose Sandstone" by M. Friedman and J. M. Logan, 15 June 1969, 43 p.

2. "Triaxial Compression Testing at Intermediate Strain Rates" by J. M. Logan and J. Handin, 15 November 1970, 28 p.

3. "Photomechanical Model Studies Relating to Fracture and Residual Elastic Strain in Granular Aggregates" by J. J. Gallagher, 15 February 1971, 127 p.

4. "Fracture-Surface Energy of Rocks" by M. Friedman, J. Handin, and G. Alani, 15 September 1970, 24 p.

5. "Geological Aspects of Residual Elastic Strain in Rocks" by M. Friedman, 15 December 1971, 53 p.

6. "Deformations Associated with Relaxation of Residual Stresses in the Barre Granite of Vermont" by T. C. Nichols, Jr., 15 December 1971, 92 p.

7. "In Situ Measurement by Photoelastic Bar Gages" by A. Brown, 1 April 1972, 82 p.

8. "Lueders' Bands in Experimentally Deformed Sandstone and Limestone" by M. Friedman and J. M. Logan, 15 September 1972, 30 p.

9. "Theory of Spacing of Extension Fracture" by G. M. Sowers, 31 December 1972, 69 p.

List of Publication

1. Brown, A. (1970) Measurement of recoverable strain in rocks from Llano, Texas, and Cody, Wyoming (Abstract): Geol. Soc. America, Abstracts with Programs, v. 2, p. 273.

2. Brown, A. (1972) In situ strain at Sandy, Blanco Co., Texas (Abstract): Am. Geophys. Union Trans., v. 53, p. 524.

3. Friedman, M. (1971) X-ray analysis of residual elastic strains in quartzose rocks, p. 573-595 in Gray, K. E., Editor, Proc. 10th Symp. Rock Mechanics: Austin, Texas, May 1968.

4. Friedman, M. (1972) Residual elastic strain in rocks, p. 563-569 in Proc. 24th Intern. Geol. Cong. Sec. 3: Montreal, Canada, August 1972.

5. Friedman, M. (1972) Geologic aspects of residual elastic strain in rocks: Tectonophysics, v. 15, p. 297-330.

6. Friedman, M. and Logan, J. M. (1969) The influence of residual elastic strain on induced fractures in three quartzose sandstones (Abstract): Am. Geophys. Union Trans., v. 50, p. 324.

7. Friedman, M. and Logan, J. M. (1970) The influence of residual elastic strain on the orientation of experimental fractures in three quartzose sandstones: Jour. Geophys. Research, v. 75, p. 387-405.

8. Friedman, M. and Logan, J. M. (1970) Microscopic feather fractures: Geol. Soc. America Bull., v. 81, p. 3417-3420.

9. Friedman, M., Logan, J. M., and Swolfs, H. S. (1972) Lueders' bands in experimentally deformed Coconino Sandstone and Solenhofen Limestone (Abstract): Am. Geophys. Union Trans., v. 53, p. 513.

10. Friedman, M., Handin, J., and Alani, G. (1972) Fracture-surface energy of rocks: Intern. Jour. Rock Mech. Min. Sci., v. 9, p. 757-766.

11. Gallagher, J. J., Sowers, G. M., and Friedman, M. (1970) Photomechancial model studies relating to fracture in granular rock aggregates (Abstract): Geol. Soc. America, Abstracts with Programs, v. 2, p. 285.

12. Handin, J. (1969) The inelastic deformation of rocks, p. 247-254 in ARPA Seismic Coupling Conference: Stanford Research Institute, January 1968.

13. Handin, J. (1972) Rock properties, p. 5-31 in Seismic Coupling Conference: Advanced Research Projects Agency, Pub. T10-17-13-1, Washington, D. C., June 1970.

14. Logan, J. M. and Handin, J. (1971) Triaxial compression testing at intermediate strain rates, p. 167-194 in Clark, G. B., Editor, Proc. 12th Symp. Rock Mechanics: Rolla, Missouri, November 1970.

15. Sowers, G. M. (1970) Theory of spacing of extension fracture (Abstract): Geol. Soc. America, Abstracts with Programs, v. 2, p. 691.

16. Sowers, G. M. (in press) Theory of spacing of extension fracture: Proc. Rapid Excavation, Geol. Soc. America, Milwaukee, Wisconsin, November 1970.

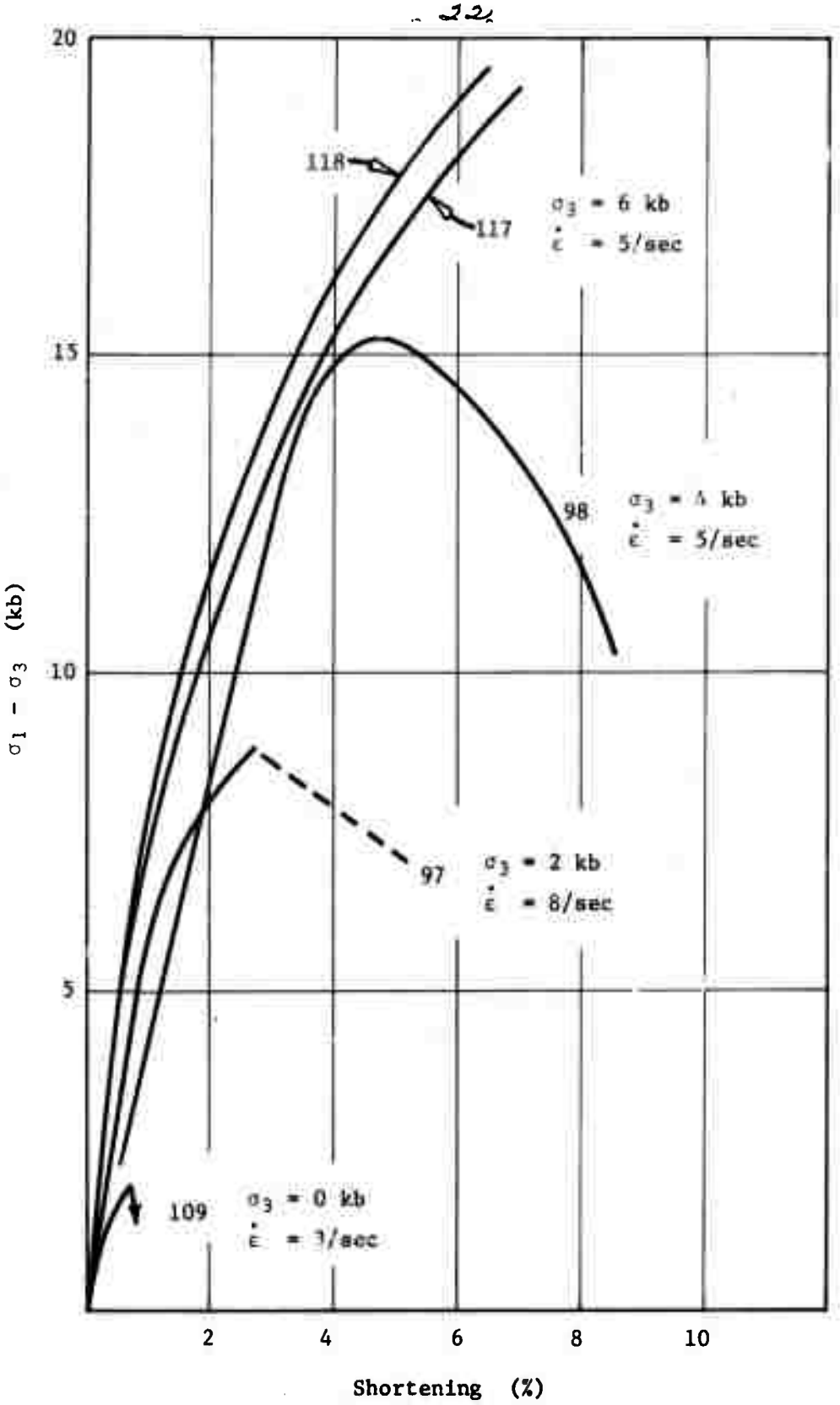

Figure 1. Stress-strain curves for Wagonwheel graywacke, deformed dry at 25°C. Confining pressure (σ_3), strain rate ($\dot{\varepsilon}$), and test number noted. Arrow denotes fracture.

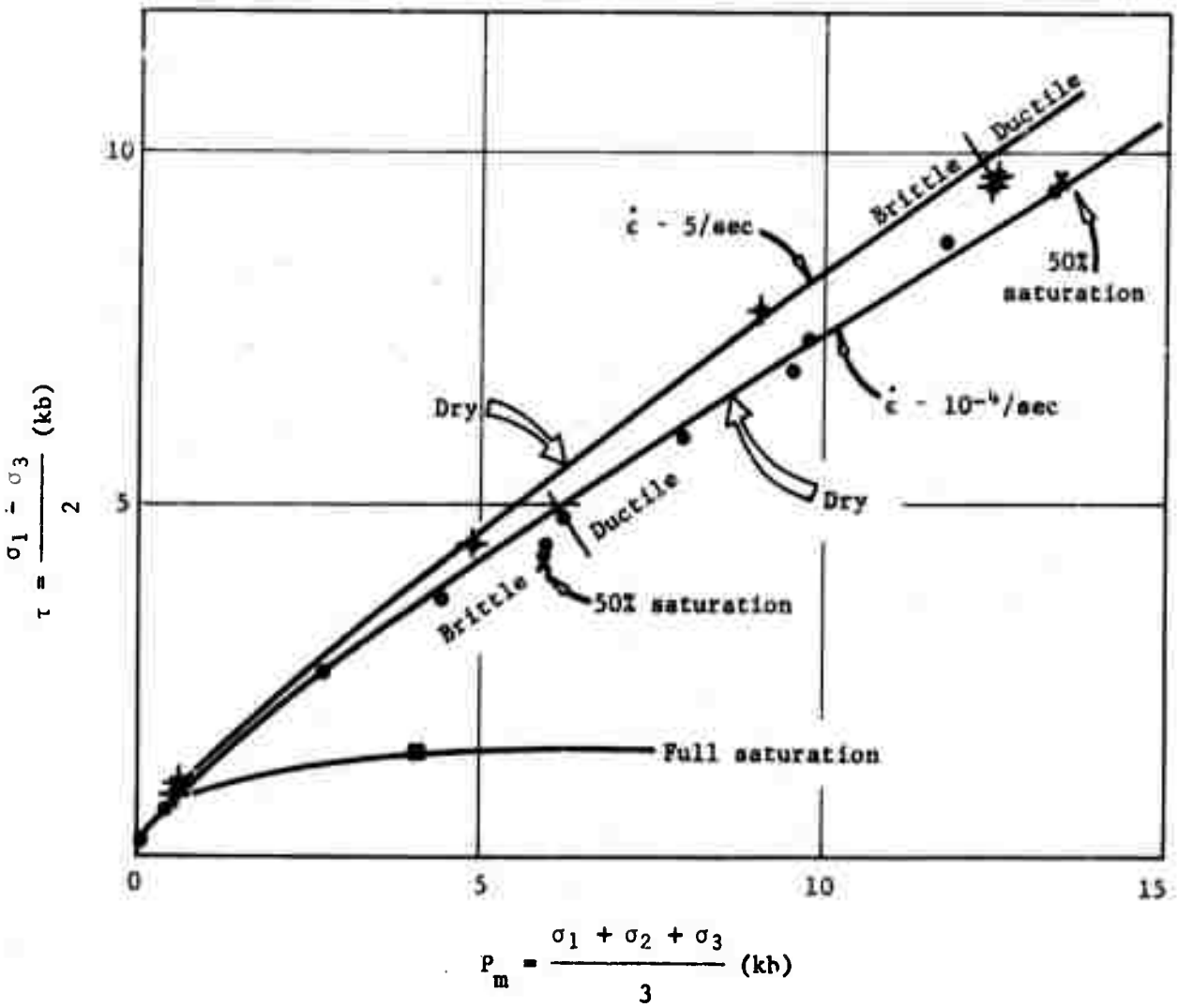

Figure 2. Maximum shear stress (τ) versus mean pressure (P_m) for Wagonwheel graywacke deformed dry, 50% saturation and full saturation, at a strain rate ($\dot{\epsilon}$) of 10^{-4}/sec, and dry at approximately 5/sec. Brittle-ductile transition shown.

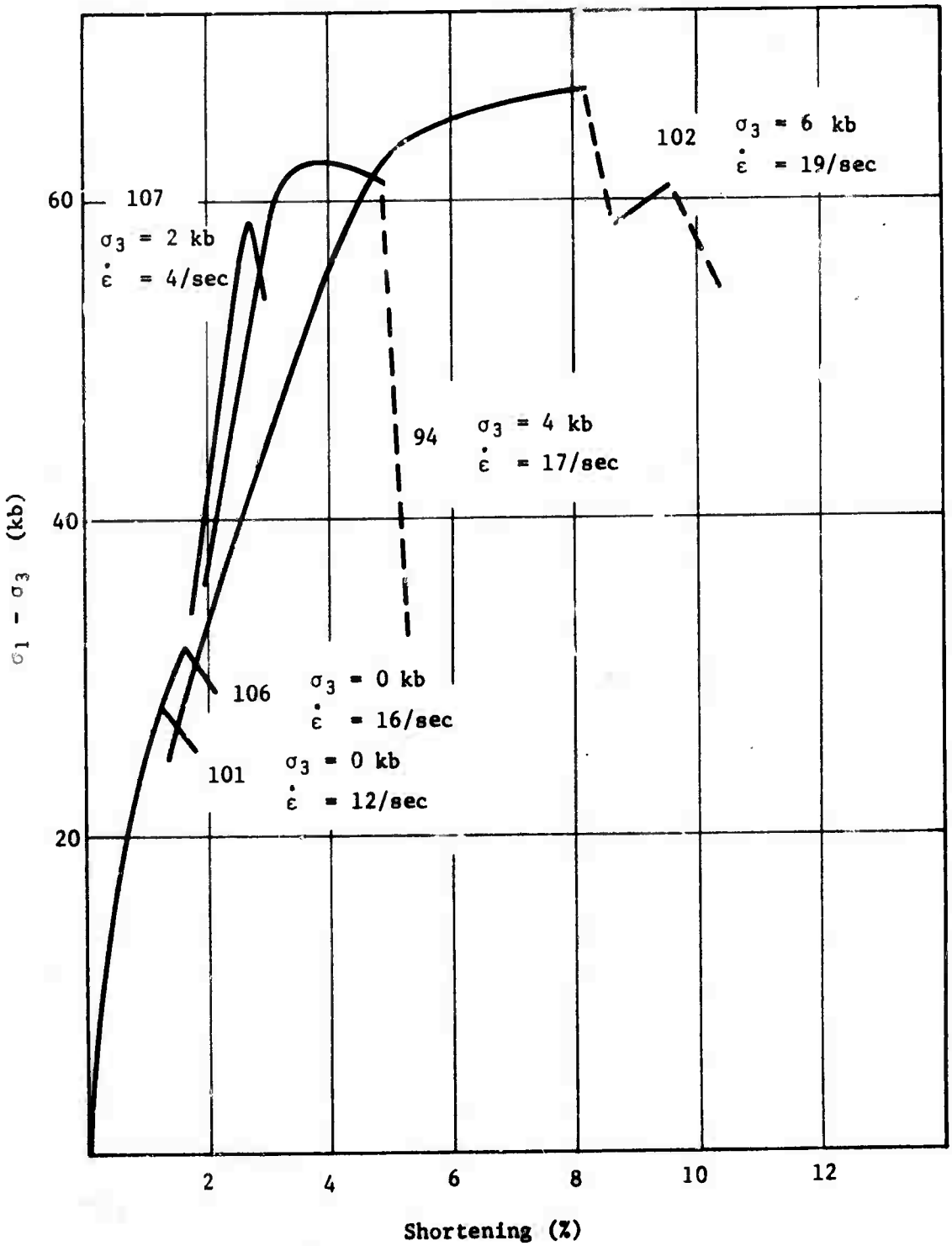

Figure 3. Stress-strain curves for beryllium oxide, cold-pressed perpendicular to plate. Specimens deformed dry, at 25°C. The confining pressures (σ_3), strain rates ($\dot{\varepsilon}$), and test numbers are noted.

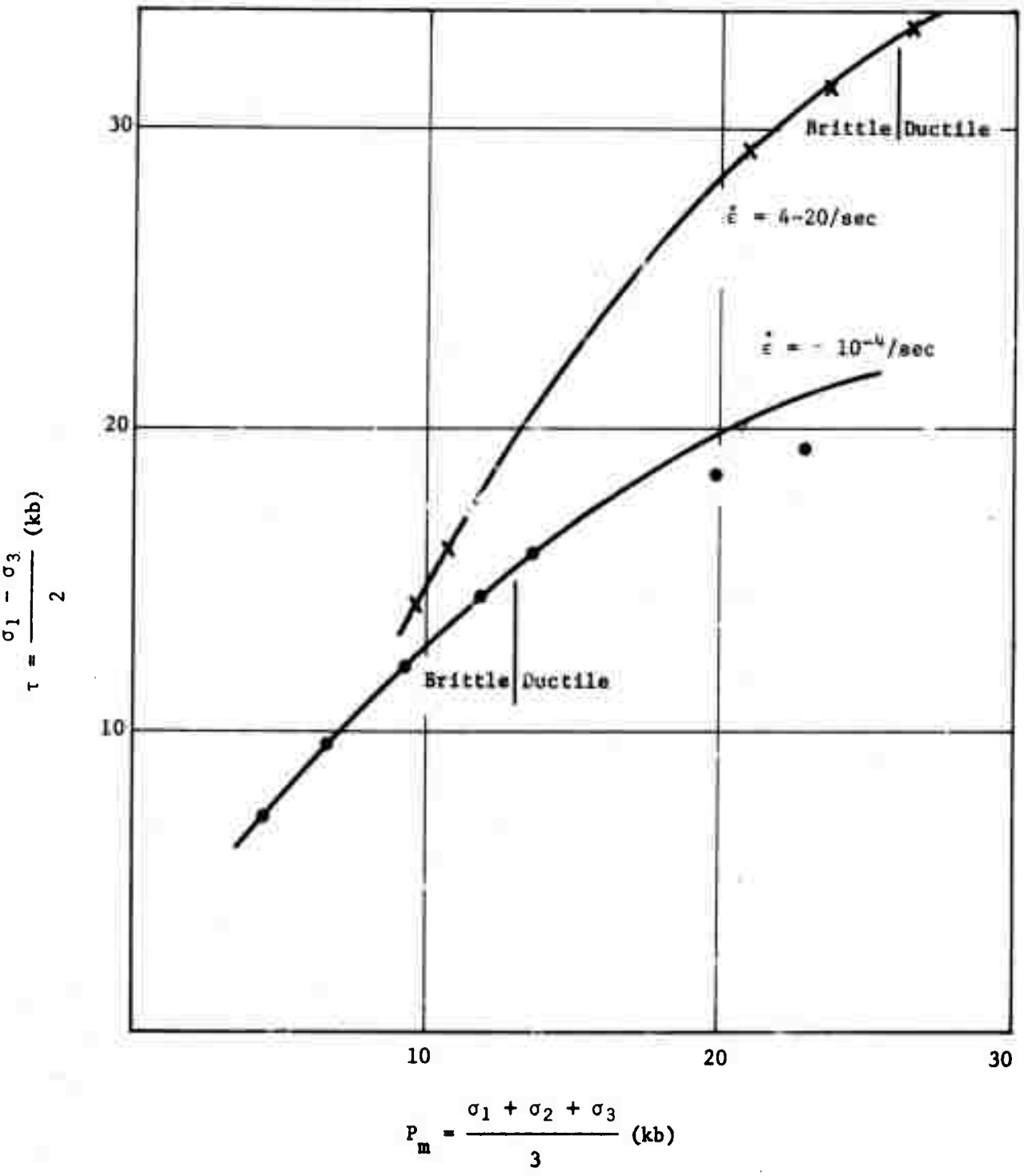

Figure 4. Maximum shear stress (τ) versus mean pressure (P_m) for cold-pressed BeO. The average strain rate ($\dot{\varepsilon}$) is shown for each curve, as is the brittle-ductile transition.

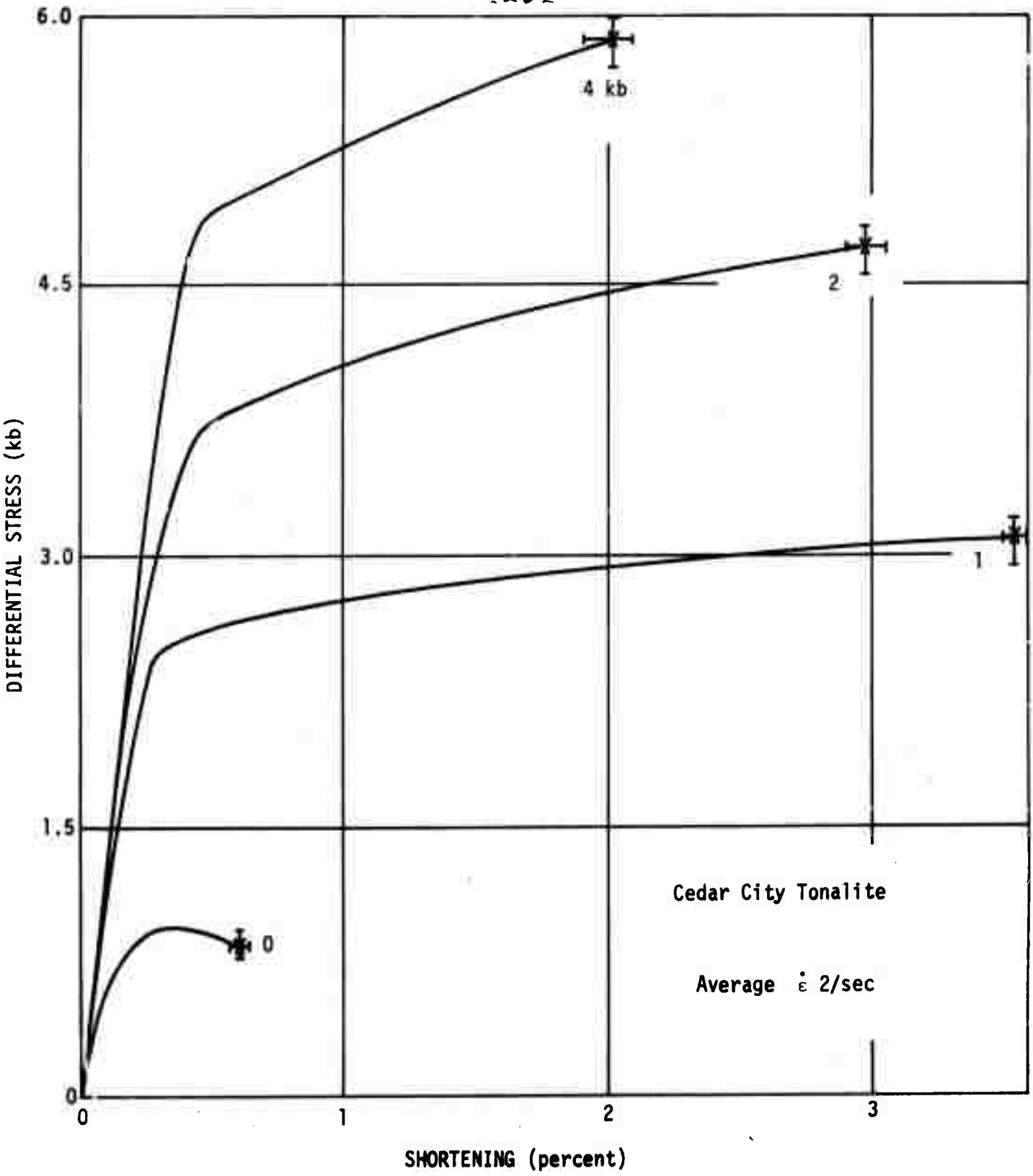

Figure 5. Stress-strain curves for dry Cedar City Tonalite. Average strain rate of 2/sec. Each curve is the average of three tests; spread of data indicated by cross. All specimens fractured.

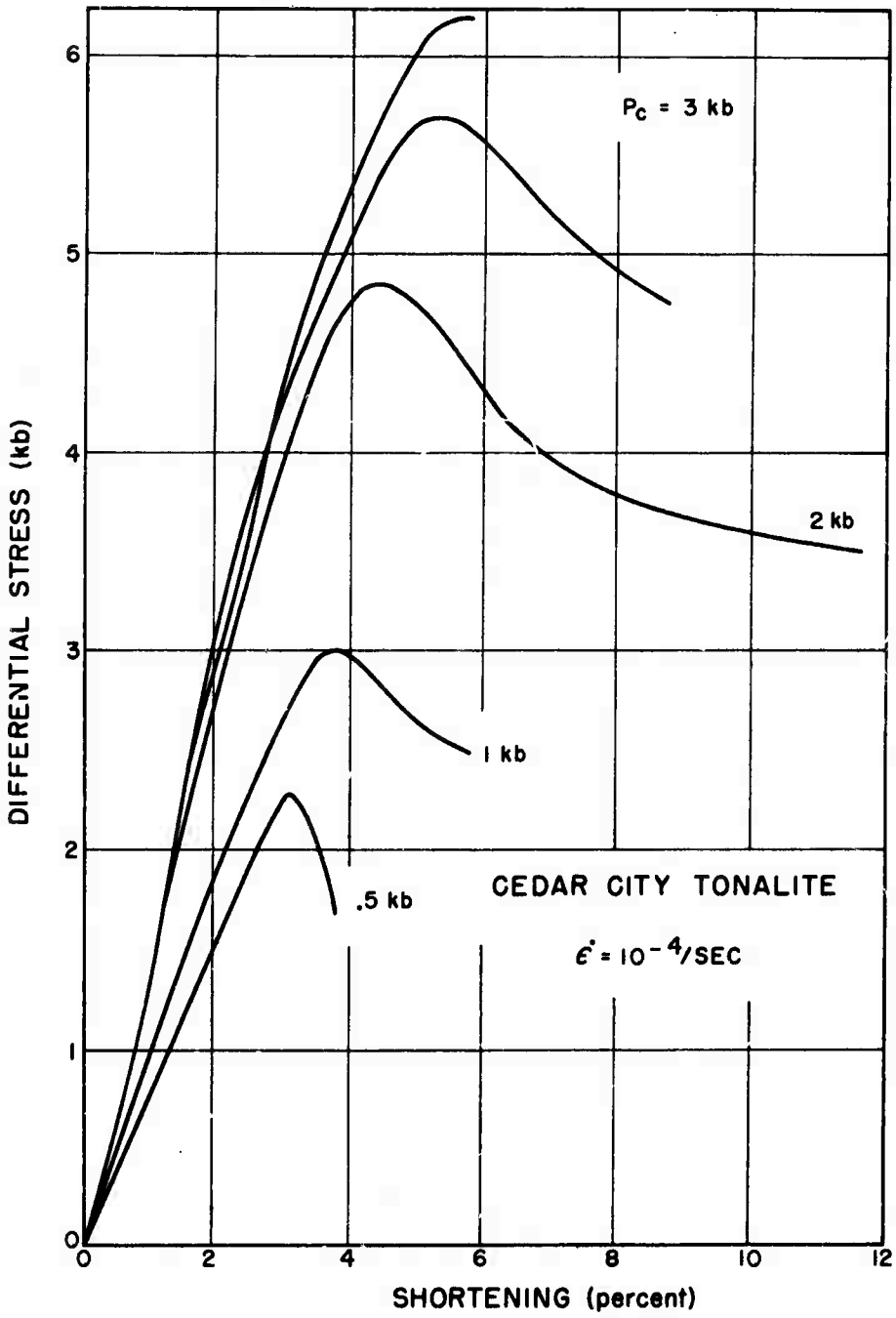

Figure 6. Stress-strain curves for dry Cedar City Tonalite deformed at a strain rate of 10^{-4}/sec. Confining pressures (kb) are indicated for each curve.

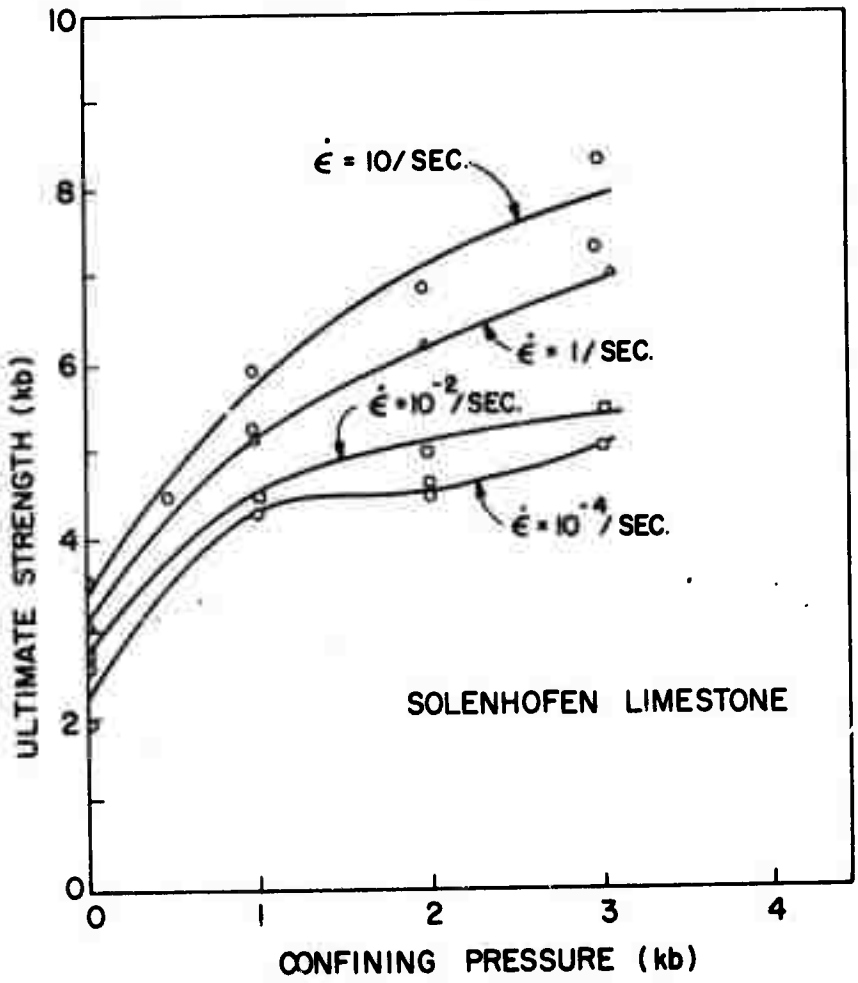

Figure 8. Ultimate strength versus confining pressure for dry Solenhofen Limestone at different strain rates ($\dot{\epsilon}$).

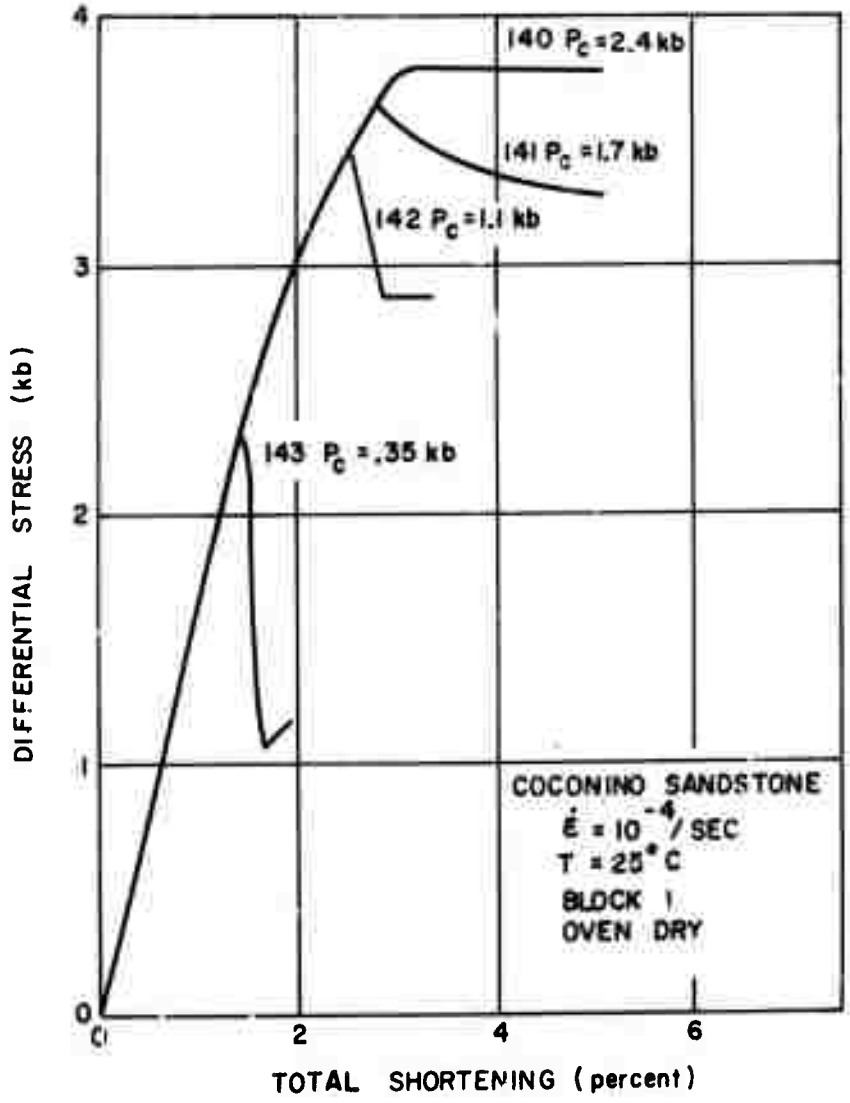

Figure 9. Stress-strain curves for dry Coconino Sandstone show brittle-ductile transition and increased ultimate strength with increasing confining pressure (P_c).

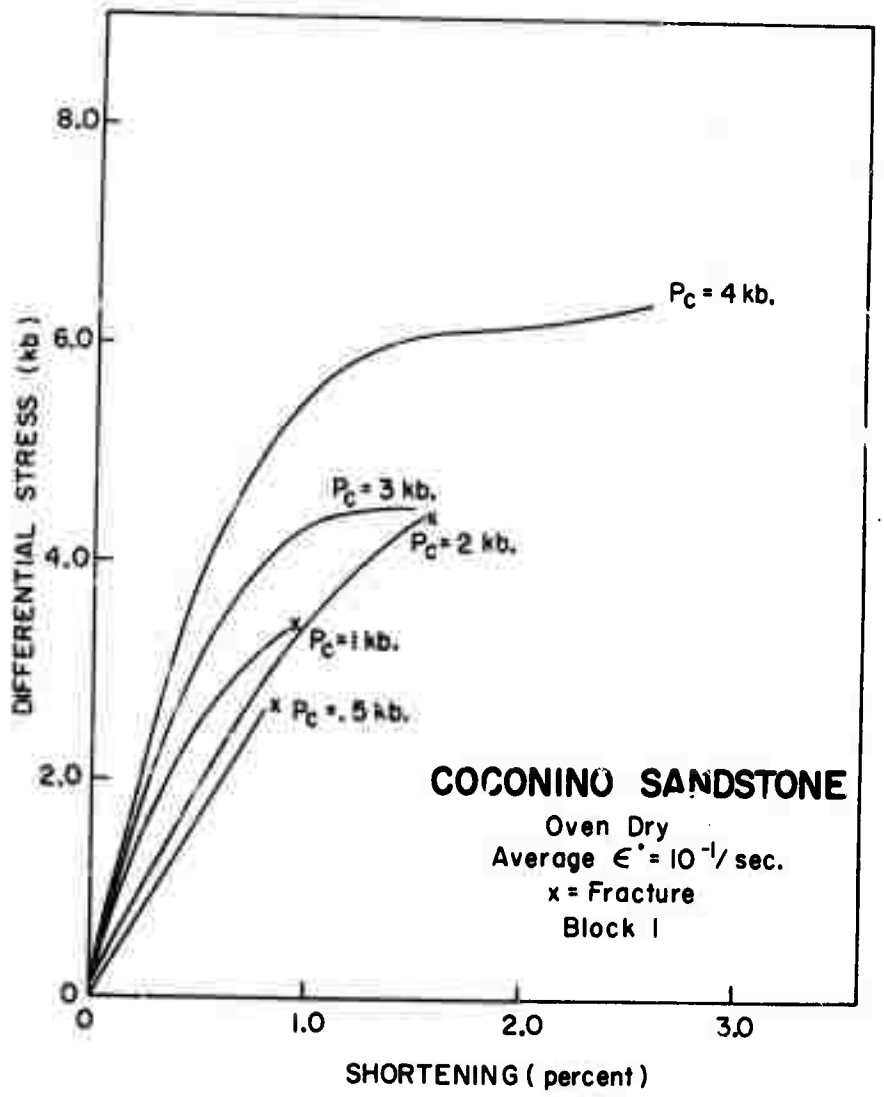

Figure 10. Stress-strain curves for dry Coconino Sandstone. Confining pressure (P_c) shown for each experiment. Strain rate ($\dot{\epsilon}$) is 10^{-1}/sec.

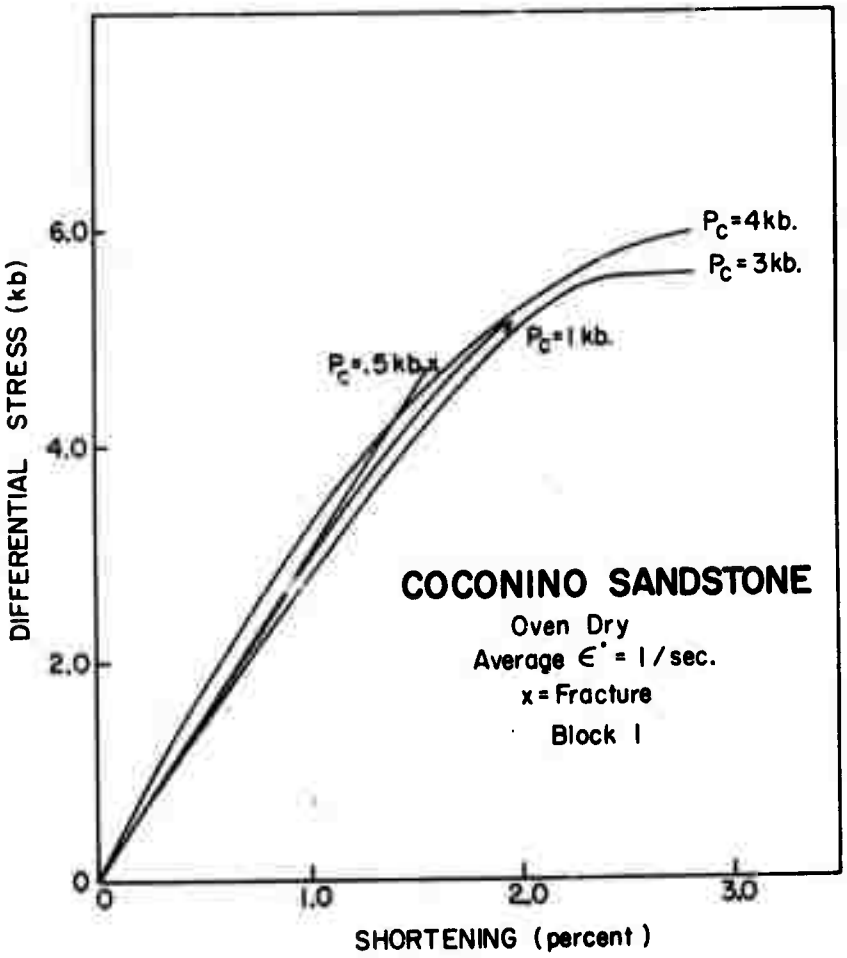

Figure 11. Stress-strain curves for dry Coconino Sandstone. Confining pressure (P_c) shown for each experiment.

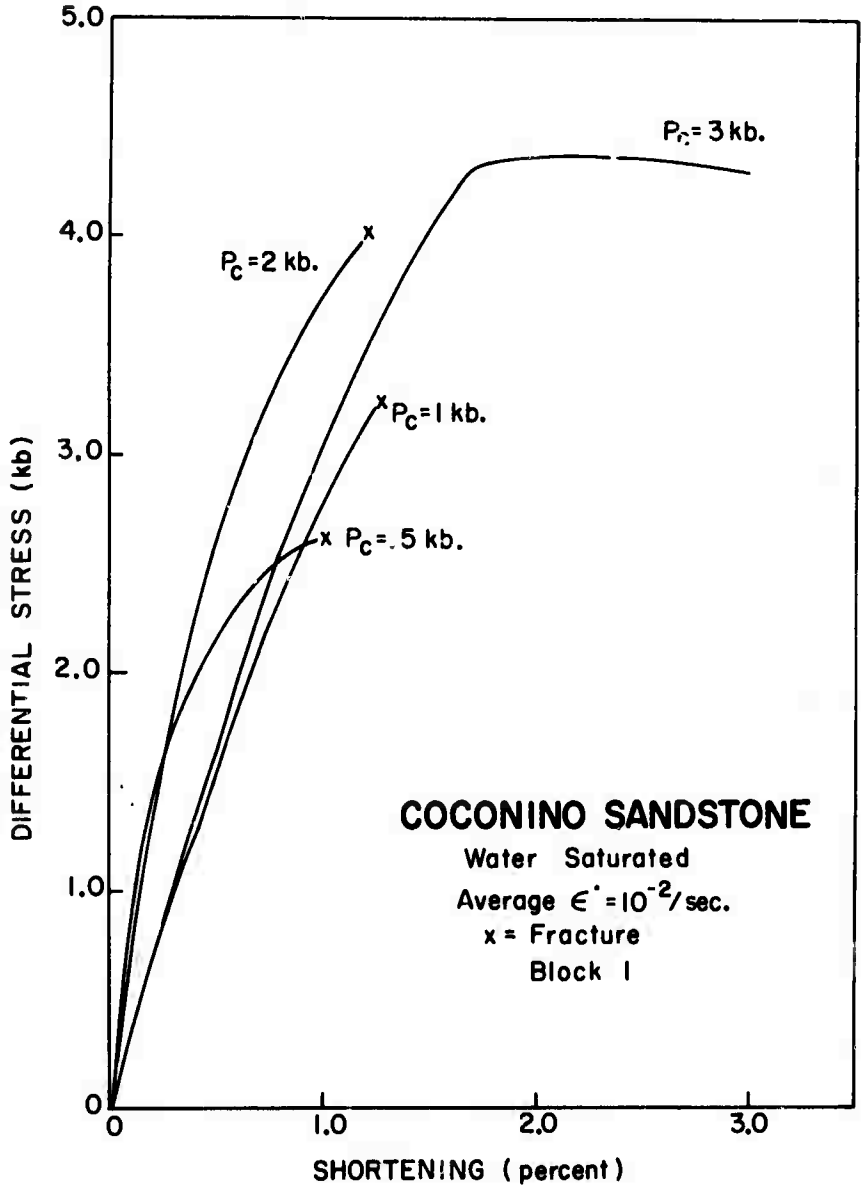

Figure 12. Stress-strain curves for water-saturated Coconino Sandstone. Confining pressure (P_c) shown for each curve.

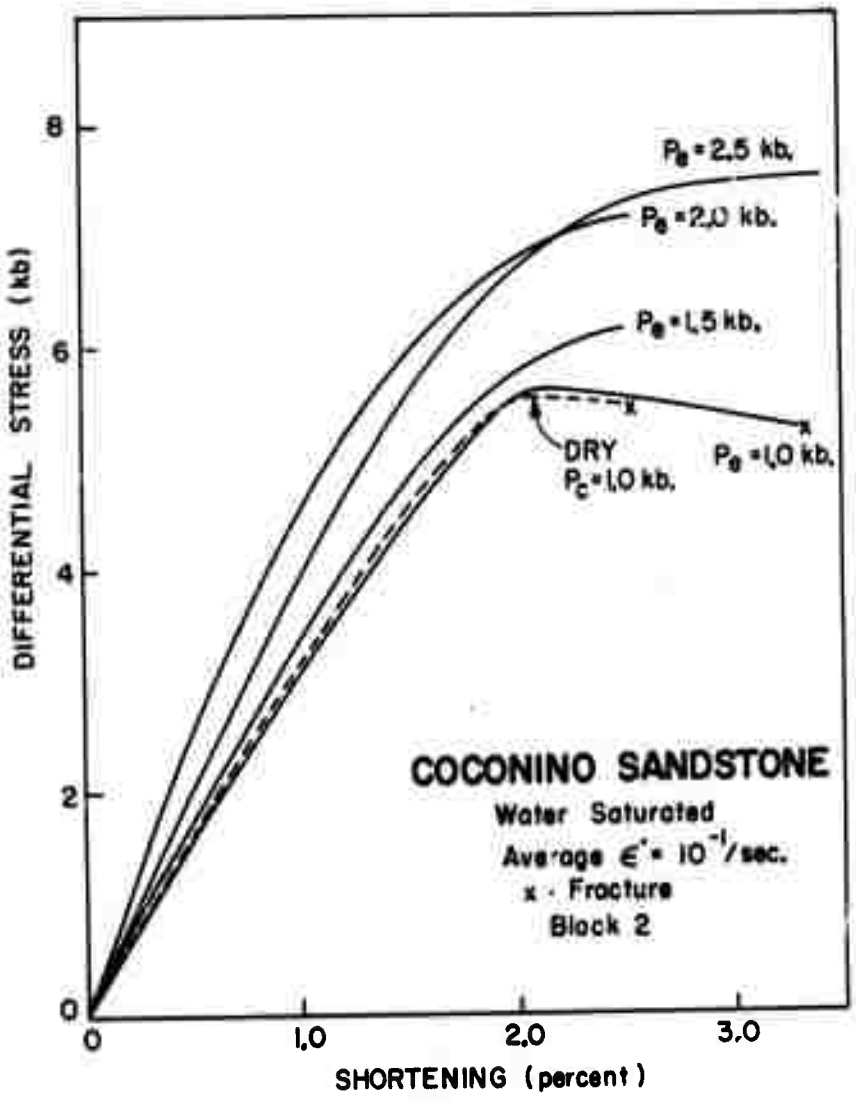

Figure 13. Stress-strain curves for water-saturated Coconino Sandstone. Effective confining pressure (P_e) shown for each experiment.